Salt-inducible kinase 3 regulates the mammalian circadian clock by destabilizing PER2 protein

Naoto Hayasaka[1,2,3*], Arisa Hirano[4], Yuka Miyoshi[3], Isao T. Tokuda[5], Hikari Yoshitane[4], Junichiro Matsuda[6], Yoshitaka Fukada[4]

1) Department of Neuroscience II, Research Institute of Environmental Medicine (RIEM), Nagoya University, Furo-Cho, Chikusa-Ku, Nagoya 464-8601, Japan

2) PRESTO, Japan Science and Technology Agency (JST), 4-1-8 Honcho, Kawaguchi, Saitama 332-0012, Japan

3) Department of Anatomy and Neurobiology, Kindai University Faculty of Medicine, 377-1 Ohno-dai, Osaka-Sayama, Osaka 589-8511, Japan

4) Department of Biological Sciences, Graduate School of Science, The University of Tokyo, 7-3-1 Hongo, Bunkyo-Ku, Tokyo 113-0033, Japan

5) Department of Mechanical Engineering, Ritsumeikan University, 1-1-1 Nojihigashi, Kusatsu, Shiga 525-8577, Japan

6) Laboratory of Animal Models for Human Diseases, National Institutes of Biomedical Innovation, Health and Nutrition, 7-6-8 Saito-Asagi, Ibaraki, Osaka 567-0085, Japan

*Corresponding author:
Naoto Hayasaka, Ph.D.
Department of Neuroscience II
Research Institute of Environmental Medicine (RIEM)
Nagoya University
Furo-Cho, Chikusa-Ku, Nagoya 464-8601, Japan
Phone: +81-52-789-3864
Fax: +81-52-789-3889

E-mail: naotohayasaka@yahoo.co.jp

Abstract

Salt-inducible kinase 3 (SIK3) plays a crucial role in various aspects of metabolism, as well as in skeletal development. In the course of investigating metabolic defects in the *Sik3*-deficient mice (*Sik3*$^{-/-}$), we observed that circadian rhythmicity of the metabolisms was phase-delayed. *Sik3*$^{-/-}$ mice also displayed other abnormalities in circadian rhythms, including lengthening of the period, impaired entrainment to the light-dark cycle, phase variation in locomotor activities, and aberrant physiological rhythms. *Ex vivo* suprachiasmatic nucleus slices from *Sik3*$^{-/-}$ mice exhibited destabilized and desynchronized molecular rhythms among individual neurons. In cultured cells, *Sik3*-knockdown resulted in cycle-to-cycle fluctuations of the circadian periodicity. Expression levels of PER2, an essential clock protein, were elevated in *Sik3*-knockdown cells but down-regulated in *Sik3*-overexpressing cells, which could be ascribed to a phosphorylation-dependent decrease in PER2 protein stability. Collectively, our results indicate that SIK3 plays key roles in murine circadian rhythms by facilitating phosphorylation-dependent destabilization of PER2.

Introduction

Circadian rhythms in mammals are governed by the master oscillator located in the hypothalamic suprachiasmatic nucleus (SCN). A growing body of evidence suggests that oscillation of the circadian clock is generated by the transcriptional-translational feedback loop composed of the circadian clock genes and their products, including the transcriptional activators CLOCK and brain/muscle ARNT-like protein 1 (BMAL1), and their negative regulators PERIODs (PER1/2/3) and CHRYPTOCHROMEs (CRY1/2) (Brown et al., 2012; Takahashi, 2015). These factors and their modulators contribute to determination and fine-tuning of the circadian period and the phase. For example, *Cry1* and *Cry2* knockout (KO) mice demonstrate respectively shortened and lengthened periods of the locomotor activity rhythms (van der Horst et al., 1999). *Tau*, a constitutively-active casein kinase I epsilon (CKIε) mutation in hamsters and mice, resulted in shortened circadian periods and advanced the phase in behavioral and physiological rhythms (Meng et al., 2008; Ralph and Menaker, 1988). These lines of evidence suggest that the transcriptional-translational feedback loop mediated by the clock genes, and the post-translational modification of their products, are indispensable for the circadian clock machinery. However, the molecular mechanisms underlying the determination or stabilization of circadian period and phase remain to be investigated in mammals.

Previous reports have suggested that protein kinases play important roles in the regulation of circadian clocks (Reischl and Kramer, 2011). For example, CKIε/δ phosphorylates PER1 and PER2 proteins, and promotes their proteasomal degradation

(Akashi et al., 2002; Eide et al., 2005; Meng et al., 2008). CRY1 and CRY2 is also phosphorylated by 5' AMP-activated protein kinase (AMPK) and dual-specificity tyrosine-phosphorylation-regulated kinase 1A (DYRK1A), and CRY2 is

phosphorylated by dual-specificity tyrosine-phosphorylation-regulated kinase 1A (DYRK1A), glycogen synthase kinase 3 beta (GSK3ß), and AMPK, leading to degradation via a ubiquitin-proteasomal pathway as well as intracellular localization being altered (Gao et al., 2013; Kurabayashi et al., 2010; Lamia et al., 2009). We have previously shown that mitogen-activated protein kinase (MAPK/ERK) contributes to robust circadian oscillation within individual SCN neurons (Akashi et al., 2008). Furthermore, the significance of kinases in human circadian rhythms has also been studied. Toh *et al.* reported that a point mutation in a clock gene *Per2* results in familial advanced sleep phase syndrome (FASPS) in human kindred (Toh et al., 2001). FASPS is an inherited abnormal sleep pattern in which the circadian clock is phase-advanced by around four hours. The *Per2* mutation causes hypophosphorylation of PER2 protein by casein kinase Iε (CKIε). CKIε requires another priming kinase for phosphorylation, which is yet to be identified. Overall, these data suggest that posttranslational modifications of clock proteins by a series of protein kinases play critical roles in regulation of the circadian clock. In the current study, we focused on salt-inducible kinase 3 (SIK3) because we found abnormal circadian rhythmicity on metabolism while we were studying *Sik3* knockout (KO) mice (Uebi et al., 2012). SIK1–3 are Ser/Thr kinase members of AMPK family, which is known as an energy sensor and regulates various aspects of metabolism in both vertebrates and invertebrates (Katoh et al., 2004;

Wang et al., 2011). Previous studies suggest critical roles of mammalian SIK3 in the metabolism of glucose, cholesterol and bile acid, and in retinoid metabolism and skeletal development (Sasagawa et al., 2012; Uebi et al., 2012). *Sik3*$^{-/-}$ mice exhibit severe metabolic symptoms such as hypolipidemia and hypoglycemia, and die very frequently on the first day after birth (Uebi et al., 2012). Furthermore, they exhibit severe defects in chondrocyte hypertrophy, expanded growth plate or cartilage, accumulation of chondrocytes, and impaired skull bone formation (Sasagawa et al., 2012). In the present study, we found that *Sik3* KO mice also demonstrate abnormal circadian phenotypes, which are similar in part, but distinct form those of CKI mutants.

Results

Sik3$^{-/-}$ mice exhibit abnormal circadian rhythms in physiology and behavior

While studying metabolic phenotypes in *Sik3*$^{-/-}$ mice, we observed that average oxygen consumption rhythm, representing circadian rhythmicity of metabolism, was significantly phase-delayed by approximately 6 h as compared to wild-type (WT) littermates (Fig. 1a). We also found that other physiological rhythms related to rectal temperature and food consumption were phase-delayed to similar degrees (Fig. 1b, c). These data raised the possibility that SIK3 plays a role in the circadian clock machinery. To examine whether *Sik3* mRNA is expressed in the hypothalamic SCN, the central circadian oscillator, we performed *in situ* hybridization on mouse brain sections (Supplementary Fig. 1), and found that *Sik3* mRNA is expressed in the SCN (Supplementary Fig. 1a, arrowhead). SIK3 protein expression in the SCN was also confirmed by immunohistochemistry (Supplementary Fig. 1b). We then performed

behavioral analysis of the *Sik3*$^{-/-}$ mice and WT (*Sik*$^{+/+}$) littermates. In 12-hour light-dark (LD) cycle conditions (LD 12:12), *Sik*$^{+/+}$ mice displayed nocturnal activity profiles in which they were entrained to the LD cycle, with activity onset at light-off (ZT12, zeitgeber time representing light-on as ZT0 and light-off as ZT12 in LD 12:12 conditions) and the activity offset at light-on (ZT0). In stark contrast, *Sik3*$^{-/-}$ mice failed to become completely entrained to the LD cycle, although they did still retain nocturnality (Fig. 1d, upper panels). Their activity onset and offset in the LD cycle did not correspond exactly to the light-off and light-on times respectively, and they fluctuated significantly with regard to light-on/light-off. These data suggest that *Sik3*$^{-/-}$ mice have a defect in a light-input pathway. In constant dark (DD) conditions, the free-running period of the wheel-running activity rhythms of the *Sik3*$^{-/-}$ mice (24.17 +/- 0.09 h, $n = 13$) was significantly longer than that of *Sik*$^{+/+}$ mice (23.80 +/- 0.05 h, $n = 15$) (Fig. 1d, e). The ability of *Sik3*$^{-/-}$ mice to entrain to a new LD cycle was examined by photic re-entrainment experiments, where mice kept in DD conditions were transferred to an LD cycle, the phase of which was shifted substantially from the free-running activity rhythm. While the free-running locomotor rhythms of *Sik*$^{+/+}$ mice rapidly re-entrained to the new LD cycle, in contrast *Sik3*$^{-/-}$ mice showed slower re-entrainment (Fig. 1d, lower panels). Even after 2 weeks in the new LD cycle, we still observed a component of the free-running rhythm formed under the DD condition (red dotted line in Fig. 1d, lower right panel) although the majority of the locomotor rhythm components were entrained to the LD condition. We then compared the acrophase of the activities of individual *Sik3*$^{-/-}$ and *Sik*$^{+/+}$ mice in LD (Fig. 1f). Acrophase means did

not differ significantly between the two genotypes, but the individual variation (standard deviation) in the acrophase distribution in *Sik3*$^{-/-}$ mice was significantly greater than that of *Sik*$^{+/+}$ mice ($p < 0.001$, F-test). These data indicated that SIK3 plays a crucial role in photic entrainment in addition to controlling and sustaining circadian behavioral rhythmicity. Notably, *Sik3*$^{-/-}$ mice were relatively less active at night than *Sik*$^{+/+}$ mice, and more active during the day, which resulted in lower amplitude in the locomotor activity rhythms (Fig. 1d, g).

Molecular rhythms are desynchronized and circadian periods and phases are varied in *ex vivo* SCN

In order to explore how SIK3 deficiency affects the circadian clocks in the SCN and periphery, *Sik3*$^{-/-}$ mice were crossed with *Per2::Luciferase* knockin (KI) mice (*Per2-luc*$^{+/+}$) expressing PER2-luciferase fusion protein in place of PER2, which monitors the circadian oscillation of PER2-luciferase fusion protein both in SCN explants and in cultured cells (Yoo et al., 2004). Brain slices including the SCN were prepared from *Sik3*$^{-/-}$ *Per2-luc*$^{+/+}$ double-homozygous mice for *ex vivo* bioluminescence imaging at the single-cell level (Fig. 2). As previously reported (Akashi et al., 2008; Fukuda et al., 2011; Yoo et al., 2004), *Sik*$^{+/+}$ SCN explants exhibited robust circadian bioluminescence rhythms and the individual cells were well synchronized with each other (Fig. 2a, d, Supplementary video 1). In contrast, the circadian periods and phases of the individual cells in *Sik3*$^{-/-}$ SCN slices were varied and their bioluminescence rhythms became gradually desynchronized with time (Fig. 2e, h, Supplementary video

2). To further evaluate the difference in the SCN rhythms between the two genotypes, we performed quantitative analyses on the periods and phases of the imaging data (Fig. 2a–h). The number of oscillating cells in *Sik3*$^{-/-}$ SCN, calculated as the percentage of oscillating pixels within the SCN, was significantly lower than that of *Sik*$^{+/+}$ controls (95.87% in *Sik*$^{+/+}$ SCN vs. 83.25% in *Sik3*$^{-/-}$ SCN, $p < 0.1$, chi-square periodogram). Although the average periods of the individual SCN cells in the *Sik3*$^{-/-}$ and *Sik*$^{+/+}$ slices were comparable to each other, the variation (standard deviation) was significantly greater in the *Sik3*$^{-/-}$ cells than in the *Sik*$^{+/+}$ cells (Fig. 2b, f, i, $p < 0.0001$, F-test). Similarly, the average acrophases of the *Per2-luc* rhythms of individual SCN cells were comparable between the two genotypes, but the variation in the *Sik3*$^{-/-}$ cells was significantly greater than that in the *Sik*$^{+/+}$ cells (Fig. 2c, g, j, $p < 0.0001$, F-test). Overall, our data demonstrated that *Sik3* deficiency reduced the number of oscillating cells and impaired the circadian rhythmicity of oscillating cells, *i.e.*, it was associated with instability in circadian period and phase, and desynchrony among SCN cells.

In vitro Sik3-knockdown destabilizes circadian periods

Fluctuation of the circadian period and phase in *Sik3*$^{-/-}$ mice *in vivo* and *ex vivo* prompted us to examine whether alteration of SIK3 expression levels affected cellular circadian rhythms in culture. NIH3T3 cells were transfected with vectors expressing four different *Sik3* short-hairpin RNAs (shRNAs), and cellular rhythms were monitored via a *Bmal1-luc* reporter gene (Fig. 2k, l, Supplementary Fig. 2a). Unexpectedly, the average periods of all the *Sik3*-knockdown (*Sik3*-KD) cells were significantly shorter

than those of WT controls (Supplementary Fig. 2b). Detailed period analyses revealed that all *Sik3*-KD cells exhibited unstable circadian rhythms, in which sequential circadian periods varied on a day-to-day basis. In addition, half-periods, representing individual peak-to-trough or trough-to-peak periods, fluctuated in all the knockdown (KD) cells examined during 1 week of monitoring, with a characteristic of longer trough-to-peak period and shorter peak-to-trough period. These data suggest that cellular circadian rhythmicity is destabilized by *Sik3* deficiency (Fig. 2m, Supplementary Fig. 2c). Consistent with the *ex vivo* SCN explant data (Fig. 2i, h), these results suggest that SIK3 is involved in circadian rhythm stability.

PER2 expression levels are altered in *Sik3*-KD cells and *Sik3*-overexpressing cells

Previous reports indicate that phosphorylation-mediated modulation of clock protein stability is mediated by multiple protein kinases (Reischl and Kramer, 2011). To explore whether SIK3 modifies the phosphorylation status of the clock proteins, we performed western blotting of cellular lysates with different expression levels of SIK3. We first examined PER2 clock protein because it has multiple phosphorylation sites. In *Sik3*-overexpressing (*Sik3*-OX) NIH3T3 cells, we found a significant reduction in PER2 protein levels in *Sik3*-OX compared to control cells (non-OX, Fig. 3a, Supplementary Fig. 2a). Cells expressing the constitutive-active SIK3 mutant T163E (Katoh et al., 2006), exhibited significantly reduced PER2 protein level in HEK293T17 cells (Fig. 3a) and NIH3T3 cells (Supplementary Fig. 3), whereas in cells expressing the kinase-deficient SIK3 mutant K37M (Katoh et al., 2006), PER2 protein levels were comparable

to those of *Sik3*-OX cells (Fig. 3a, Supplementary Fig3). This suggests that the kinase activity of SIK3 is required for PER2 destabilization. Remarkably, we observed that the relative level of the up-shifted PER2 band (relative to the total of the PER2 bands) was elevated in *Sik3*-OX cells as compared to non-OX controls (Fig. 3b, Supplementary Fig. 4b). Protein phosphatase (λPPase) treatment reduced these up-shifted PER2 bands, which confirmed that the shifted bands were phosphorylated forms of PER2 (Fig. 3c). We further investigated whether *Sik3*-OX induced PER2 instability or degradation. When protein synthesis was inhibited by treatment with cycloheximide (CHX), we observed a rapid decrease in PER2 levels in SIK3-OX cells as compared to the control cells, suggesting that SIK3 accelerates PER2 degradation (Fig. 3d, Supplementary Fig. 4b). To confirm SIK3-mediated phosphorylation-dependent degradation of PER2, we employed four different types of *Sik3*-KD cells, and examined both PER2 abundance and its phosphorylation status. All four *Sik3*-KD cell-types expressing different *Sik3* shRNAs exhibited elevated levels of PER2 protein (Figs. 3e, Supplementary Fig. 5a, b), and the relative levels of the up-shifted PER2 bands were significantly reduced (Fig. 3f, Supplementary Fig. 5c). λPPase treatment of these cells resulted in reduction of the up-shifted PER2 protein (Fig. 3g). Degradation of PER2 protein levels in any of the *Sik3*-KD cells was significantly delayed, for as long as 6 h after CHX treatment (Fig. 3h). These data strongly suggest that SIK3 regulates PER2 abundance and stability through its phosphorylation.

Phosphorylation and degradation of PER2 by SIK3 through a CKI-independent

pathway

SIK3-catalyzed phosphorylation of PER2 was examined via an *in vitro* kinase assay. The up-shifted band of PER2 was significantly increased after incubation of PER2 with SIK3, and the total amount of PER2 was reduced in a manner dependent on the amount of SIK3 added (Fig. 4a). An *in vitro* phosphatase/kinase assay, on the other hand, demonstrated that the down-shifting effect of phosphatase pre-treatment on the PER2 band was counteracted by the addition of SIK3 (Fig. 4b). When PER2 was treated with λPPase after incubation with SIK3, the up-shifted PER2 band was significantly reduced, confirming that the up-shifted band was a form of PER2 that was phosphorylated by SIK3 (Fig. 4c).

As mentioned above, CKI is known to phosphorylate PER2 and induce PER2 degradation through proteasomal pathway (Akashi et al., 2002; Eide et al., 2005; Meng et al., 2008). It has also been reported that CKI requires an unidentified priming kinase prior to phosphorylate its substrates (Gallego and Virshup, 2007). To address the question of whether SIK3 phosphorylation of PER2 is independent of phosphorylation by CKI (Akashi et al., 2002; Eide et al., 2005; Meng et al., 2008), NIH3T3 cells co-transfected with *Per2* and *Sik3* were incubated with the CKI inhibitor IC261, or the proteasome inhibitor MG132. Neither of the inhibitors affected PER2 degradation by SIK3, confirming that SIK3-dependent PER2 degradation is independent of CKI-mediated PER2 degradation through a proteasome pathway (Fig. 4d). Conversely, KD of *Sik3* had no significant effect on the CKI-mediated phosphorylation states of PER2 (Fig. 4e). Taken together, these data indicated that PER2 phosphorylation via two

different kinases, CKI and SIK3, are independent events.

Discussion

In the current study, we found that SIK3-mediated phosphorylation of PER2 regulates the abundance of the protein by accelerating its degradation. Interestingly, while both CKIε/δ and SIK3 phosphorylate PER2 and promote its degradation, the underlying mechanisms appear to differ from each other. However, two questions remain: how do they share or divide roles in terms of the regulation of PER2 stability and abundance, and why are two kinases that induce distinct degradation systems required for a common substrate? To address these questions, it is worth noting that *Sik3*$^{-/-}$ mice exhibit unique circadian phenotypes compared to those of *Tau* mutants, although both of these mutants also have features in common. While *Tau* mice, constitutively active *CKIε* mutants, demonstrate significant phase advance and shorter periods in physiological and behavioral rhythms (Meng et al., 2008; Ralph and Menaker, 1988), *Sik3*$^{-/-}$ mice, which are loss-of-function mutants, exhibit significant phase delay and longer circadian periods as shown in the current study (Fig. 1). It has also been reported that *CKIδ* KO liver exhibits significantly longer period in *Per2-luc* rhythms (Etchegaray et al., 2009). These data suggest that both SIK3 and CKI contribute to precise circadian period determination, and that deficiency of either protein results in period shortening along with stabilization of PER2. On the other hand, unique circadian phenotypes observed in *Sik3*$^{-/-}$ mice included: (i) fluctuating circadian periods and phases both *in vivo* (Fig. 1a–f) and *in vitro* (Fig. 2), (ii) impaired light-entrainment (Fig. 1d), (iii) reduced amplitude in locomotor activity rhythm (Fig. 1g), and (iv)

desynchrony of rhythmicity among SCN cells (Fig. 2d, h, Supplementary video 1, 2), none of which have been reported in *CKI* mutants except that reduced amplitude in *Per2-luc* rhythms were observed in *CKIδ* KO liver (Etchegaray et al., 2009). Consequently, our present . Thus, the data from the current study suggest that while CKI is involved in determination of precise circadian period length and phase, SIK3 is more important for stabilization of circadian periods and phase via intercellular coupling, as well as for photic entrainment (Fig. 4f). In other words, while the two kinases may have an overlapping role or roles with regard to phosphorylating and destabilizing PER2, SIK3 and CKI contribute differentially to circadian clock regulation.

It is also interesting to note that the above-described phenotypic differences between *Tau* mutants and *Sik3*$^{-/-}$ mice may be at least partly explained by differential roles of the two protein kinases outside of the SCN. For example, SIK3 is expressed in the eye (Lizcano et al., 2004) as well as in the SCN, and hence disruption of this gene may affect the circadian light-input pathway involving the retina, which is critical for photic-entrainment. SIK3 is also known to play a role in various aspects of metabolism, and *Sik3*$^{-/-}$ mice exhibit significantly lower blood sugar levels (Uebi et al., 2012). This could result in lower amplitude of behavioral rhythms, as they must feed intermittently even in the resting period (daytime).

It has previously been shown that constitutive expression of *Per2* causes arrhythmia *in vitro* and *in vivo* (Chen et al., 2009; Yamamoto et al., 2005). This might partly explain the aberrant rhythmicity in *Sik3*$^{-/-}$ mice due to accumulation of PER2 protein. Desynchrony among SCN cells, which has been observed in circadian rhythm

mutants (Maywood et al., 2006), may lead to insufficient light-entrainment or inconstant behavioral rhythms. Lastly, the *Sik3* gene is highly conserved in evolution, from nematodes to mammals (Okamoto et al., 2004), and *Sik3* deficiency results in severe phenotypes such as high lethality after birth and metabolic and skeletal abnormalities (Sasagawa et al., 2012; Uebi et al., 2012). These previous studies suggest that SIK3 plays an essential role in various tissues and organs. Considering that animal behavior is influenced by physiological states, we cannot exclude the possibility that behavioral and physiological abnormalities in circadian rhythms in *Sik3*-/- mice such as those observed in the current study are due to defects not only in the SCN, but in other parts of the brain or in other organs or tissues. Conditional *Sik3*-/- mice may be a suitable tool for addressing these questions in the future.

It has been reported that SIK1, another isoform of the SIK subfamily, is involved in photic entrainment of the master circadian clock (Jagannath et al., 2013), although its involvement in the central circadian clock remains uncertain. Notably, while the present study demonstrated that SIK3 regulates photic-entrainment, light responses in behavior observed in *Sik1*-KD mice (Jagannath et al., 2013) and *Sik3*$^{-/-}$ mice are contrary to each other: rapid vs. delayed re-entrainment, respectively. In addition, the SIK3 substrate clock protein PER2, which is involved in circadian regulation, differs from the SIK1 substrate CREB-regulated transcription coactivator 1 (CRTC1) (Jagannath et al., 2013). Although further studies are necessary to elucidate the involvement of the two SIK isoforms in light-resetting mechanisms, the current study suggests that SIK3 contributes to the light-input pathway in addition to the circadian clock machinery in a manner that

differs from SIK1, by regulating different substrates and signaling pathways.

Just recently, Funato *et al.* reported that, by large-scale forward-genetics screen in mice to seek dominant sleep abnormalities, a splicing mutation of *Sik3* (referred to as a *Sleepy* mutant) resulted in significant decrease in wake time caused by extended non-REM sleep (Funato et al., 2016). In the *Sleepy* mutants in which a point mutation resulting in a lack of a protein kinase A (PKA) recognition site of the SIK3 protein, the authors also indicated that locomotor activity rhythms in the mutants were normal. Although the results were in contrast with our present data, the discrepancy could be explained by difference in introduced mutations; i.e., a partial deletion in the *Sleepy* mutants versus null mutation in our *Sik3* KO mice.

Acknowledgements

We are grateful to Hiroshi Takemori and Minako Koura for providing *Sik3* KO mice, Joseph Takahashi for providing *Per2-luc* KI mice, and Daisuke Ono, Sato Honma, and Ken-Ichi Honma for providing bioluminescence imaging data. We also thank Mamoru Nagano, Yuka Sugahara, Mika Machida and Nana Itou for technical assistance.

Additional information

Competing interests

Authors have declared that no competing interests exist.

Funding

1. Funder: Grant-in-Aid for Scientific Research from the Japan Society for the Promotion of Science (JSPS). Grant Reference number: No. 25293053, 21590264. Author: Naoto Hayasaka.
2. Funder: The PRESTO Program from Japan Science and Technology Agency (JST). Author: Naoto Hayasaka.

The funders had no role in study design, data collection and interpretation, or the decision to submit the work for publication.

Author contributions

N.H. designed the research. N.H., A.H., and Y.F. wrote the manuscript. N.H., A.H., Y.M., I.T.T., and H.Y. performed experiments, and N.H., A.H., I.T.T., H.Y. and Y.F. analyzed data. J.M. provided materials and intellectual guidance throughout the project, and assisted with the generation of the initial manuscript.

Ethics

Animal experimentation: This study was performed in strict accordance with the recommendations in the Guide for the Care and Use of Laboratory Animals of the Japan Society for Promotion of Sciences. All of the animals were handled according to approved institutional animal care and use committee of each university/institution.

References

Akashi, M., Hayasaka, N., Yamazaki, S., and Node, K. (2008). Mitogen-activated protein kinase is a functional component of the autonomous circadian system in the suprachiasmatic nucleus. J Neurosci 28, 4619-4623.

Akashi, M., Tsuchiya, Y., Yoshino, T., and Nishida, E. (2002). Control of intracellular dynamics of mammalian period proteins by casein kinase I epsilon (CKIepsilon) and CKIdelta in cultured cells. Molecular and cellular biology 22, 1693-1703.

Brown, S.A., Kowalska, E., and Dallmann, R. (2012). (Re)inventing the circadian feedback loop. Developmental cell 22, 477-487.

Chen, R., Schirmer, A., Lee, Y., Lee, H., Kumar, V., Yoo, S.H., Takahashi, J.S., and Lee, C. (2009). Rhythmic PER abundance defines a critical nodal point for negative feedback within the circadian clock mechanism. Mol Cell 36, 417-430.

Doi, M., Okano, T., Yujnovsky, I., Sassone-Corsi, P., and Fukada, Y. (2004). Negative control of circadian clock regulator E4BP4 by casein kinase Iepsilon-mediated phosphorylation. Curr Biol 14, 975-980.

Eide, E.J., Woolf, M.F., Kang, H., Woolf, P., Hurst, W., Camacho, F., Vielhaber, E.L., Giovanni, A., and Virshup, D.M. (2005). Control of mammalian circadian rhythm by CKIepsilon-regulated proteasome-mediated PER2 degradation. Molecular and cellular biology 25, 2795-2807.

Etchegaray, J.P., Machida, K.K., Noton, E., Constance, C.M., Dallmann, R., Di Napoli, M.N., DeBruyne, J.P., Lambert, C.M., Yu, E.A., Reppert, S.M., et al. (2009). Casein kinase 1 delta regulates the pace of the mammalian circadian clock. Molecular and cellular biology 29, 3853-3866.

Fukuda, H., Tokuda, I., Hashimoto, S., and Hayasaka, N. (2011). Quantitative analysis of phase wave of gene expression in the mammalian central circadian clock network. PloS one 6, e23568.

Funato, H., Miyoshi, C., Fujiyama, T., Kanda, T., Sato, M., Wang, Z., Ma, J., Nakane, S., Tomita, J., Ikkyu, A., et al. (2016). Forward-genetics analysis of sleep in randomly mutagenized mice. Nature 539, 378-383.

Gallego, M., and Virshup, D.M. (2007). Post-translational modifications regulate the ticking of the circadian clock. Nature reviews Molecular cell biology 8, 139-148.

Gao, P., Yoo, S.H., Lee, K.J., Rosensweig, C., Takahashi, J.S., Chen, B.P., and Green, C.B. (2013). Phosphorylation of the cryptochrome 1 C-terminal tail regulates circadian period length. The Journal of biological chemistry 288, 35277-35286.

Halberg, F., Tong, Y. L., Johnson, E. A. (1967). Circadian System Phase - An Aspect of Temporal Morphology (Berlin: Springer-Verlag).

Jagannath, A., Butler, R., Godinho, S.I., Couch, Y., Brown, L.A., Vasudevan, S.R., Flanagan, K.C., Anthony, D., Churchill, G.C., Wood, M.J., et al. (2013). The CRTC1-SIK1 pathway regulates entrainment of the circadian clock. Cell 154, 1100-1111.

Katoh, Y., Takemori, H., Horike, N., Doi, J., Muraoka, M., Min, L., and Okamoto, M. (2004). Salt-inducible kinase (SIK) isoforms: their involvement in steroidogenesis and adipogenesis. Molecular and cellular endocrinology 217, 109-112.

Katoh, Y., Takemori, H., Lin, X.Z., Tamura, M., Muraoka, M., Satoh, T., Tsuchiya, Y., Min, L., Doi, J., Miyauchi, A., et al. (2006). Silencing the constitutive active transcription factor CREB by the LKB1-SIK signaling cascade. FEBS J 273, 2730-2748.

Kurabayashi, N., Hirota, T., Sakai, M., Sanada, K., and Fukada, Y. (2010). DYRK1A and glycogen synthase kinase 3beta, a dual-kinase mechanism directing proteasomal degradation of CRY2 for circadian timekeeping. Molecular and cellular biology 30,

1757-1768.

Lamia, K.A., Sachdeva, U.M., DiTacchio, L., Williams, E.C., Alvarez, J.G., Egan, D.F., Vasquez, D.S., Juguilon, H., Panda, S., Shaw, R.J., et al. (2009). AMPK regulates the circadian clock by cryptochrome phosphorylation and degradation. Science 326, 437-440.

Lizcano, J.M., Goransson, O., Toth, R., Deak, M., Morrice, N.A., Boudeau, J., Hawley, S.A., Udd, L., Makela, T.P., Hardie, D.G., et al. (2004). LKB1 is a master kinase that activates 13 kinases of the AMPK subfamily, including MARK/PAR-1. EMBO J 23, 833-843.

Maywood, E.S., Reddy, A.B., Wong, G.K., O'Neill, J.S., O'Brien, J.A., McMahon, D.G., Harmar, A.J., Okamura, H., and Hastings, M.H. (2006). Synchronization and maintenance of timekeeping in suprachiasmatic circadian clock cells by neuropeptidergic signaling. Curr Biol 16, 599-605.

Meng, Q.J., Logunova, L., Maywood, E.S., Gallego, M., Lebiecki, J., Brown, T.M., Sladek, M., Semikhodskii, A.S., Glossop, N.R., Piggins, H.D., et al. (2008). Setting clock speed in mammals: the CK1 epsilon tau mutation in mice accelerates circadian pacemakers by selectively destabilizing PERIOD proteins. Neuron 58, 78-88.

Okamoto, M., Takemori, H., and Katoh, Y. (2004). Salt-inducible kinase in steroidogenesis and adipogenesis. Trends Endocrinol Metab 15, 21-26.

Ralph, M.R., and Menaker, M. (1988). A mutation of the circadian system in golden hamsters. Science 241, 1225-1227.

Reischl, S., and Kramer, A. (2011). Kinases and phosphatases in the mammalian

circadian clock. FEBS Lett 585, 1393-1399.

Sasagawa, S., Takemori, H., Uebi, T., Ikegami, D., Hiramatsu, K., Ikegawa, S., Yoshikawa, H., and Tsumaki, N. (2012). SIK3 is essential for chondrocyte hypertrophy during skeletal development in mice. Development 139, 1153-1163.

Sokolove, P.G., and Bushell, W.N. (1978). The chi square periodogram: its utility for analysis of circadian rhythms. J Theor Biol 72, 131-160.

Takahashi, J.S. (2015). Molecular components of the circadian clock in mammals. Diabetes, obesity & metabolism 17 Suppl 1, 6-11.

Toh, K.L., Jones, C.R., He, Y., Eide, E.J., Hinz, W.A., Virshup, D.M., Ptacek, L.J., and Fu, Y.H. (2001). An hPer2 phosphorylation site mutation in familial advanced sleep phase syndrome. Science 291, 1040-1043.

Uebi, T., Itoh, Y., Hatano, O., Kumagai, A., Sanosaka, M., Sasaki, T., Sasagawa, S., Doi, J., Tatsumi, K., Mitamura, K., et al. (2012). Involvement of SIK3 in glucose and lipid homeostasis in mice. PloS one 7, e37803.

van der Horst, G.T., Muijtjens, M., Kobayashi, K., Takano, R., Kanno, S., Takao, M., de Wit, J., Verkerk, A., Eker, A.P., van Leenen, D., et al. (1999). Mammalian Cry1 and Cry2 are essential for maintenance of circadian rhythms. Nature 398, 627-630.

Wang, B., Moya, N., Niessen, S., Hoover, H., Mihaylova, M.M., Shaw, R.J., Yates, J.R., 3rd, Fischer, W.H., Thomas, J.B., and Montminy, M. (2011). A hormone-dependent module regulating energy balance. Cell 145, 596-606.

Yamamoto, Y., Yagita, K., and Okamura, H. (2005). Role of cyclic mPer2 expression in the mammalian cellular clock. Molecular and cellular biology 25, 1912-1921.

Yoo, S.H., Yamazaki, S., Lowrey, P.L., Shimomura, K., Ko, C.H., Buhr, E.D., Siepka, S.M., Hong, H.K., Oh, W.J., Yoo, O.J., et al. (2004). PERIOD2::LUCIFERASE real-time reporting of circadian dynamics reveals persistent circadian oscillations in mouse peripheral tissues. Proc Natl Acad Sci U S A 101, 5339-5346.

Figure legends

Figure 1

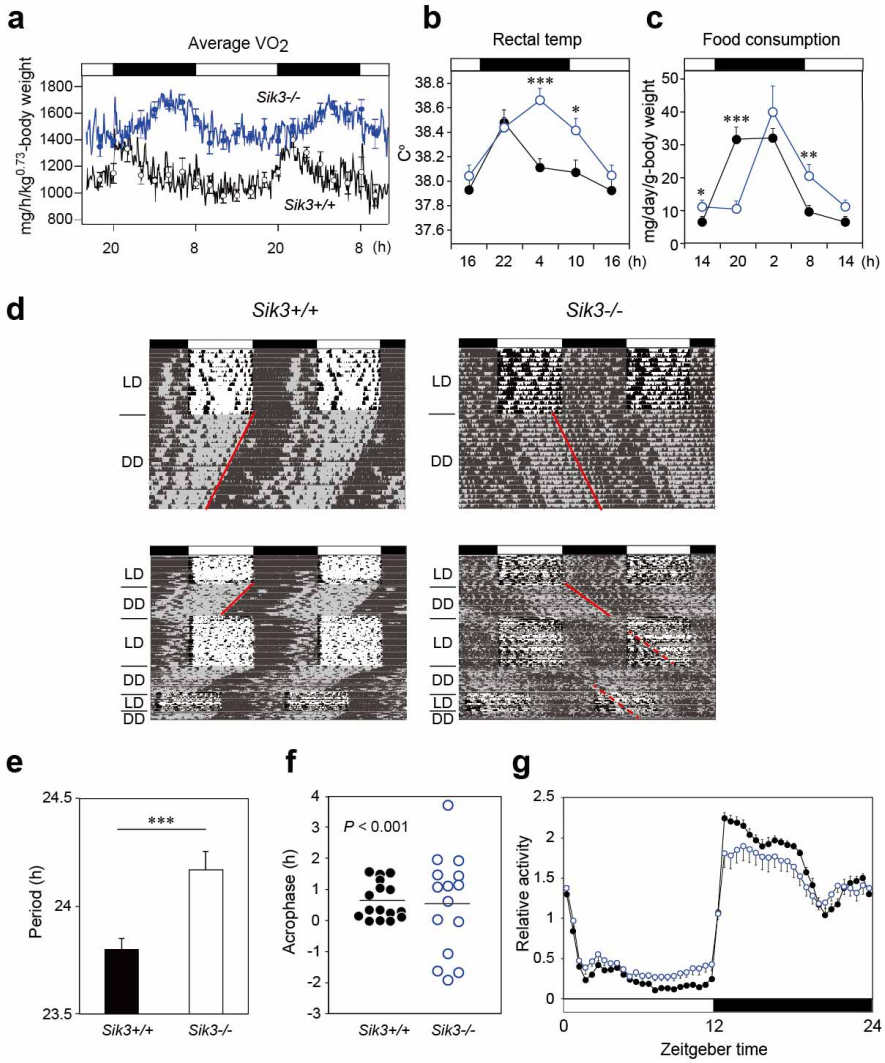

Figure 1. *Sik3*$^{-/-}$ mice exhibit aberrant circadian rhythms in physiology and behavior.

a. Oxygen consumption rhythm was measured in *Sik3*$^{-/-}$ mice and *Sik3*$^{+/+}$ controls for two days (n = 3 per group), and mean values are shown. The peak in the *Sik3*$^{-/-}$ mice (blue line) was phase-delayed by approximately 6 hours compared with that of *Sik3*$^{+/+}$ mice (black line). **b.** Rectal temperature rhythm in the *Sik3*$^{-/-}$ mice was phase-delayed (n = 3 each). **c.** Food consumption rhythm also exhibited delayed phase (n = 3 per each). Note that continuous food intake was observed in the *Sik3*$^{-/-}$ mice during the resting phase (daytime). **d.** Locomotor activity rhythms in the *Sik3*$^{-/-}$ mice and *Sik3*$^{+/+}$ controls. Upper panels demonstrate impaired entrainment to the light-dark cycles, low amplitude, variable phases, and significantly longer free-running periods in *Sik3*$^{-/-}$ mice compared to *Sik3*$^{+/+}$ controls (see angles of red lines). Lower panels show light re-entrainment experiments. In contrast to *Sik3*$^{+/+}$ mice, in which behavioral rhythms entrained to LD cycles after transition from DD to LD, it took more than 2 weeks for *Sik3*$^{-/-}$ mice to become entrained to LD. In addition, a portion of the activity rhythms in DD persistently free-ran for as long as 3 weeks after conversion from DD to LD in the *Sik3*$^{-/-}$ mice (see dotted lines). **e.** Average free-running periods in the *Sik3*$^{-/-}$ mice (n = 13) and *Sik3*$^{+/+}$ mice (n = 15). **f.** Distribution of average acrophase in individual *Sik3*$^{-/-}$ (n = 15) and *Sik3*$^{+/+}$ (n = 16) mice. $p < 0.001$ for the test for equality of variance (F-test) vs. *Sik3*$^{+/+}$. **g.** Averaged activity plots of *Sik3*$^{+/+}$ mice (black line, n = 16, average of 16 days) and *Sik3*$^{-/-}$ mice (blue line, n = 15) in LD. $*p < 0.05$, $**p < 0.01$, $***p < 0.001$ vs. *Sik3*$^{+/+}$ (Student's t-test).

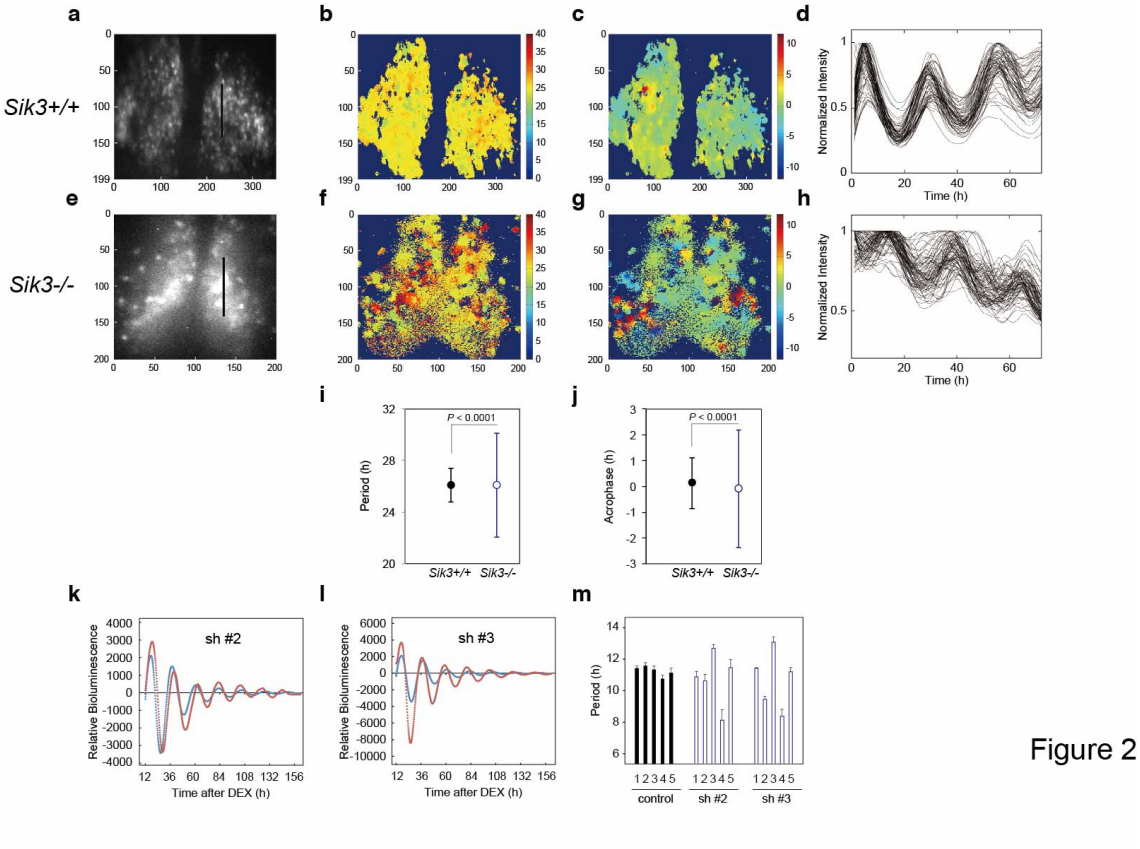

Figure 2

Figure 2. Varied circadian periods and phases in individual cells of the *Sik3*$^{-/-}$ SCN.

Time-lapse single-cell bioluminescence images of *ex vivo* SCN explant cultures of **(a)** *Sik3*$^{+/+}$ *Per2-luc*$^{+/+}$ and **(e)** *Sik3*$^{-/-}$ *Per2-luc*$^{+/+}$ mice were used for the following analyses: Period distribution on SCN slices of *Sik3*$^{+/+}$ (**b**) and *Sik3*$^{-/-}$ (**f**). Acrophase distribution on SCN slices of *Sik3*$^{+/+}$ (**c**) and *Sik3*$^{-/-}$ (**g**). Time series of the bioluminescence signals observed on a *Sik3*$^{+/+}$ SCN slice along the bold line indicated in **a** (**d**), and those from a *Sik3*$^{+/+}$ SCN slice along the bold line indicated in **b** (**h**). The original signals were smoothed via a moving average filter, and then normalized. **i.** Period distribution in representative *Sik3*$^{+/+}$ and control slices. $p < 0.0001$ vs. *Sik3*$^{-/-}$ (test for equality of variance, F-test). **j.** Acrophase distribution of representative *Sik3*$^{+/+}$ and *Sik3*$^{-/-}$ slices. $p <$ 0.0001 vs. *Sik3*$^{-/-}$ (F-test). **k** and **l.** Representative *Bmal1-luc* rhythms of *Sik3*-KD

NIH3T3 (sh #2 and #3, red) and control cells (blue). **m.** Averaged sequential half-periods (peak-to-trough or trough-to-peak) of *Bmal1-luc* rhythms in KD and control NIH3T3 cells as shown in **k** and **l** (n = 3 per group). Numbers (1–5) of the first half-period (hours from second trough to third peak) to the fifth half-period (hours from sixth trough to seventh peak) are indicated on the x-axis.

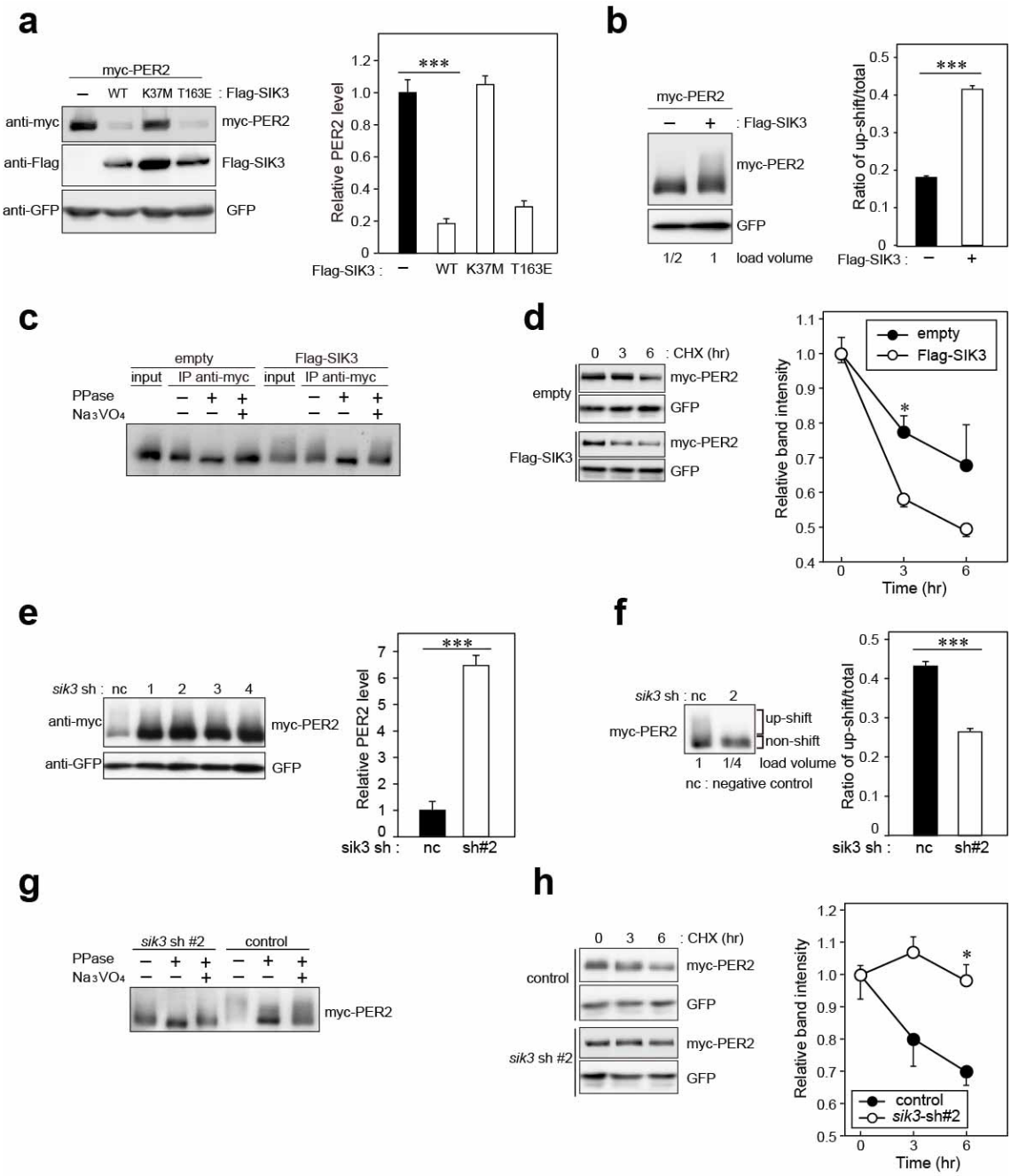

Figure 3

Figure 3. SIK3 alters expression levels and phosphorylation states of PER2 protein.

a. Western blotting revealed that overexpression of SIK3 (SIK3-OX) in HEK293T17 cells (WT) and constitutively-active SIK3 cells (T163E), but not kinase-deficient SIK3 mutant cells (K37M), significantly reduced PER2 protein levels (n = 3, $P<0.001$ by

Tukey's test). **b.** Load volume was adjusted for comparison of phosphorylation rate. Adjustment of PER2 levels in SIK3-OX and non-OX controls revealed increased rates of upshifted PER2 protein (upshift/total) in NIH3T3 cells (n = 3, ***P<0.001 vs. controls by Student's t-test). **c.** PER2 up-shift was decreased after λPPase treatment in SIK3-OX cells. **d.** *Sik3*-OX accelerated PER2 degradation. Cells were collected at 0, 3, and 6 hours after the addition of CHX. PER2 protein levels at the starting point (t=0) were normalized to 1 (n = 3, *P<0.05 by Student's t-test). **e.** Overexpression of *Sik3* shRNAs (SIK3-KD, #1–4) significantly increased PER2 levels. **f.** *Sik3*-KD reduced PER2 up-shift. (n = 3 for control and shRNA#2, ***P<0.001 vs. controls by Student's t-test). **g.** λPPase treatment reduced the phosphorylated form of PER2, and the addition of the phosphatase inhibitor Na_3VO_4 restored phospho-PER2. **h.** *Sik3*-KD suppressed degradation of PER2. PER2 protein levels at the starting point (t = 0) were normalized to 1 (n = 3, *P<0.05 by Student's t-test).

Figure 4

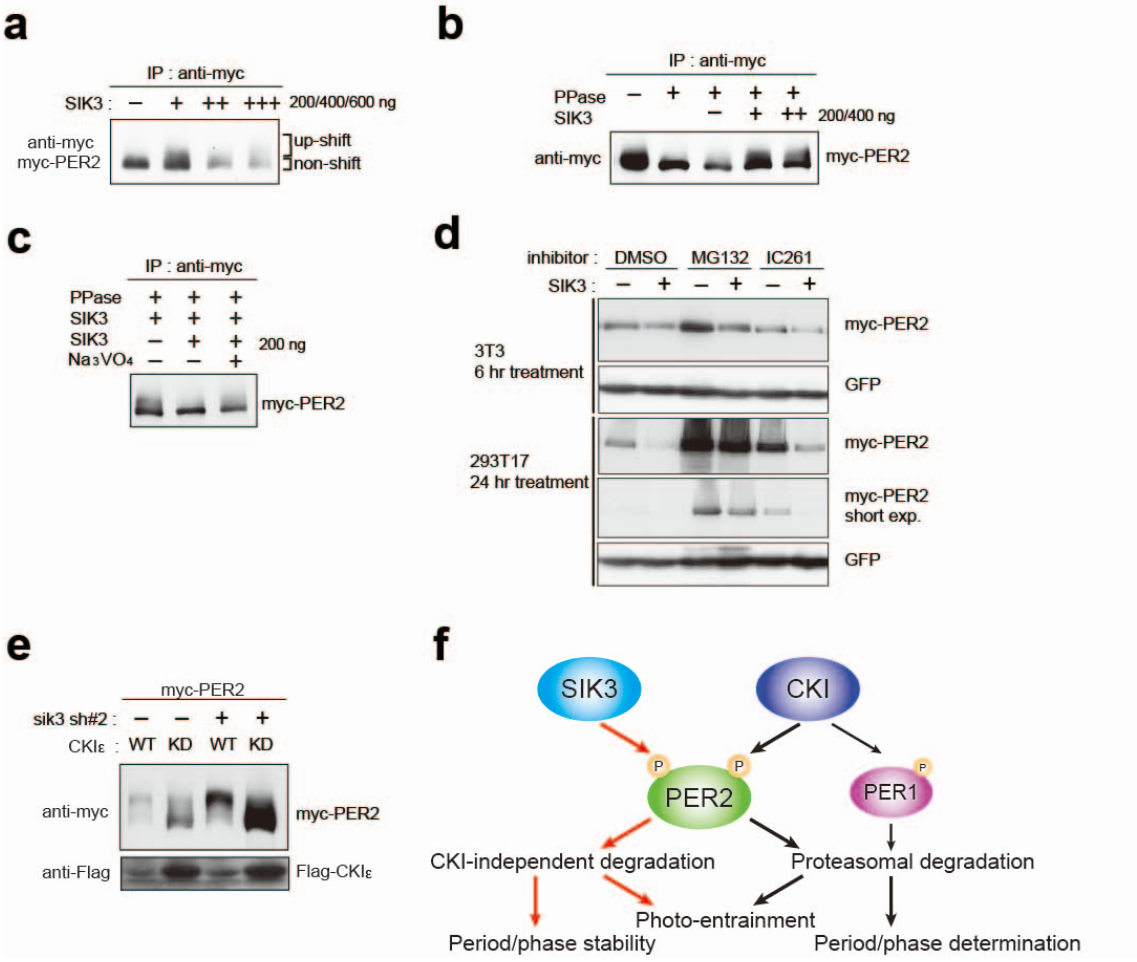

Figure 4. CKI-independent phosphorylation and destabilization of PER2 by SIK3.

a. *In vitro* kinase assays demonstrated that incubation of PER2 protein with SIK3 increased the up-shifted PER2 band, indicating that SIK3 phosphorylates PER2. **b.** Treatment of PER2 with λPPase prior to incubation with SIK3 did not affect PER2 up-shift, confirming that PER2 is phosphorylated by SIK3. **c.** Addition of λPPase after incubation of PER2 with SIK3 significantly reduced the phosphorylation of PER2. **d.**

Neither CKI inhibitor (IC261) or proteasome inhibitor (MG132), which inhibits CKI-dependent protein degradation pathway, affected SIK3-mediated PER2 phosphorylation and degradation in both NIH3T3 and HEK293T17 cells. **e.** *Sik3*-KD did not affect CKI-mediated phosphorylation or degradation of PER2 in NIH3T3 cells. **f.** A schematic representation of a potential role for SIK3 compared with that of CKI. Although both SIK3 and CKI phosphorylate PER2 protein and promote PER2 degradation, their roles and degradation pathways seems to be different. Therefore, it may not be the case that SIK3 act as a priming kinase for CKI, but the two kinases regulate PER2 independently. P represents phosphate.

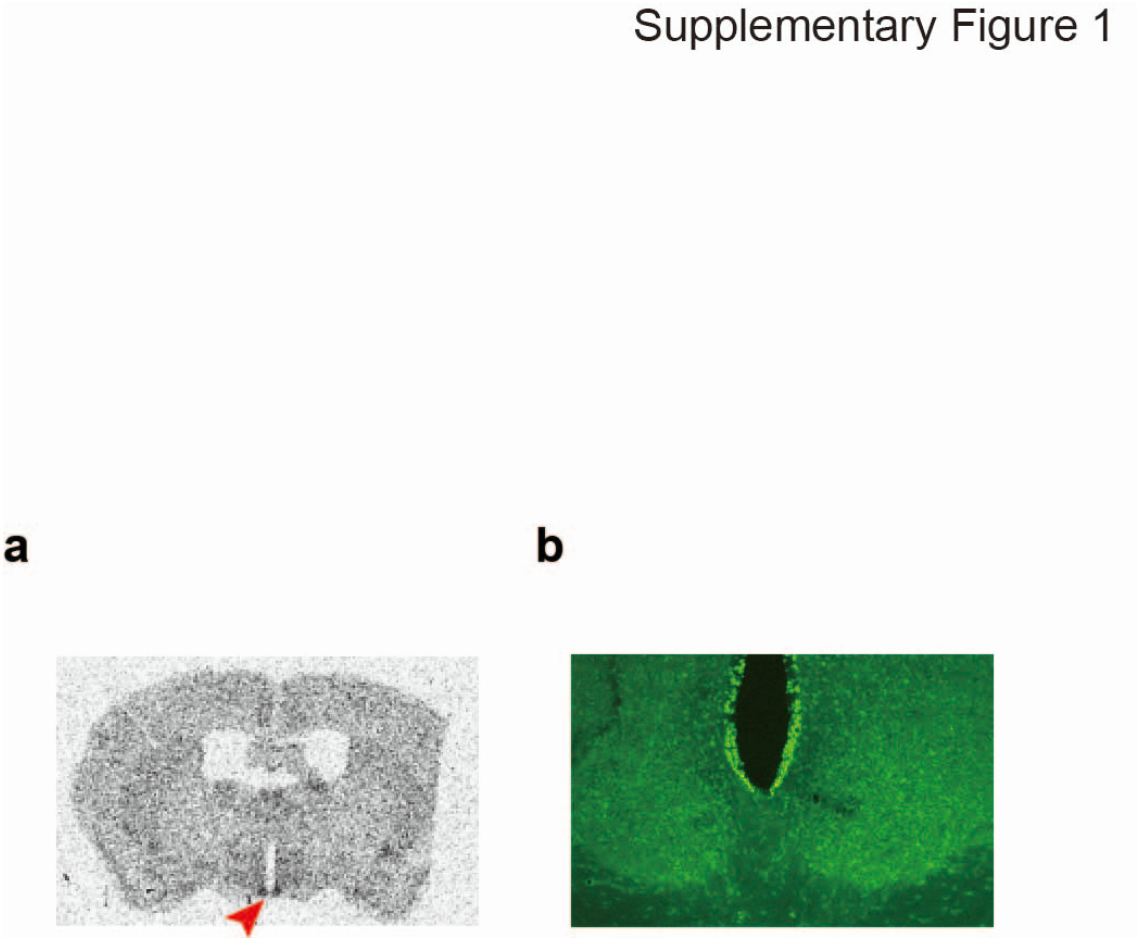

Supplementary Figure 1. Expression patterns of the *Sik3* mRNA and SIK3 protein

in the mouse brain.

a. Distribution of *Sik3* mRNA in the mouse brain as detected by *in situ* hybridization using a ^{35}S-labeled riboprobe. Note that the mRNA was expressed in almost entire areas of the brain and intense signal is observed in the SCN (arrowheads). **b.** SIK3 protein distribution in the SCN as revealed by immunohistochemistry (right panel).

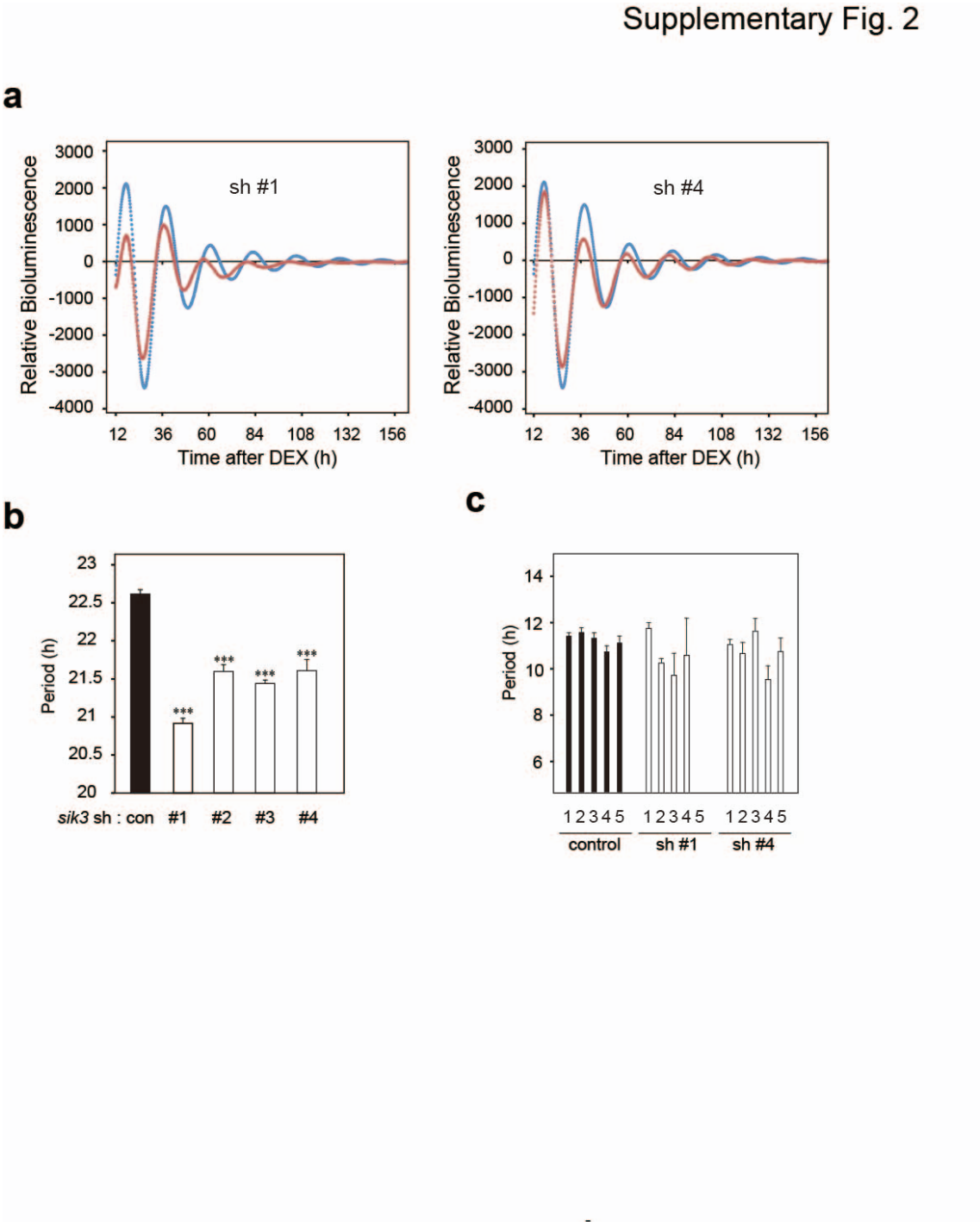

Supplementary Figure 2. *Sik3* knockdown cells exhibit shortened and unstable period of circadian *Per2-luc* rhythms

a. A representative *Bmal1-luc* bioluminescence rhythms of NIH3T3 cells transfected with *Sik3*-KD (sh #1 or sh #4, red) and control shRNA (blue) (n = 4) as shown in Fig.

2k and l. **b.** Average circadian periods of individual experiments as shown in **b** and Fig. 2k-l. (n=4, ***P<0.001 vs. controls by Dunnett's test) **c.** Average half-periods of *Sik3*-KD cells as shown in **a** (also see Fig. 2m).

Supplementary Fig. 3

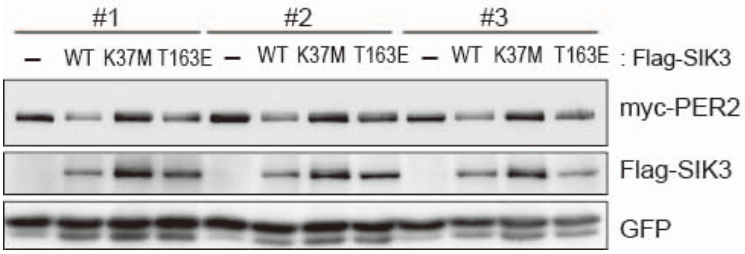

Supplementary Figure 3. Constitutive active mutant, but not kinase-deficient SIK3, alters PER2 abundance in NIH3T3 cells

Effects of WT or mutant SIK3 expression on PER2 levels were examined in NIH3T3 cells (n = 3). GFP was used for loading control.

Supplementary Fig. 4

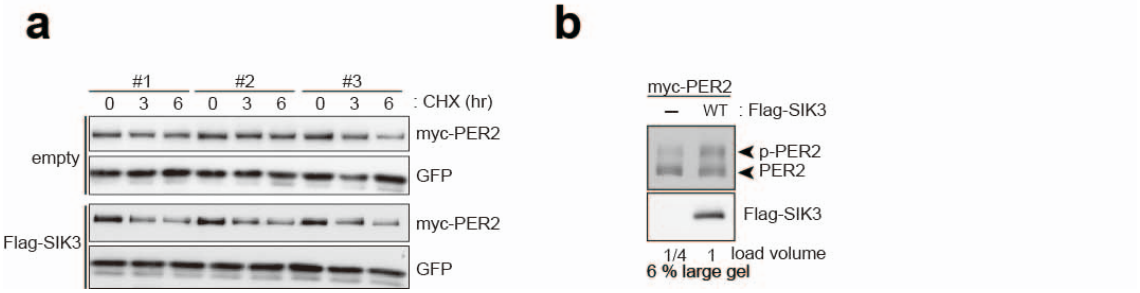

Supplementary Figure 4. Overexpression of SIK3 promotes PER2 degradation

a. Time-dependent decrease of PER2 levels by *Sik3*-OX as shown in Fig. 3d. **b.** SIK3-OX induces PER2 upshift as confirmed by co-transfection of myc-PER2 and Flag-SIK3 in HEK293T17 cells. Load volume was adjusted for comparison of phosphorylation rate.

Supplementary Fig. 5

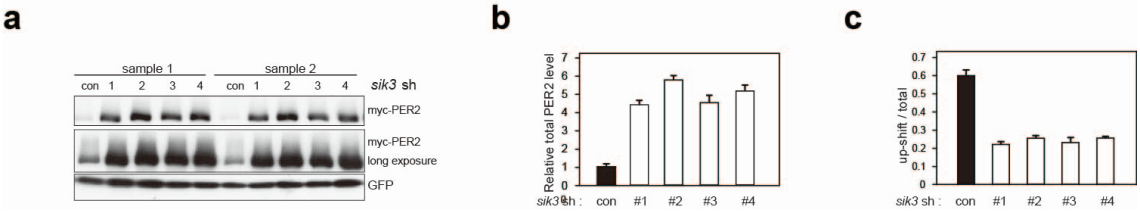

Supplementary Figure 5. *Sik3* knockdown reduces degradation of PER2 and increases its levels

a. All four different *Sik3* shRNAs increased PER2 levels as shown in Fig. 3e. **b.** Quantification of the relative total PER2 levels shown in a. Data are shown as means +SD (n=2). **c.** Quantification of phospholylated/total PER2 levels shown in a. Data are shown as means +SD (n=2).

Methods

Mice

All animals were cared for in accordance with Law No. 105 and Notification No. 6 of the Japanese Government, and experimental protocols involving the mice were approved by the relevant ethics committees at Kindai University and Nagoya University. Mice were maintained at 23 ± 1 °C under LD 12:12 or constant darkness (DD conditions). The derivation of the *Sik3*$^{-/-}$ mice has been reported previously (Uebi et al., 2012). Briefly, the PGK-neo cassette was inserted in place of exon 1 of *Sik3*. The successful targeting of embryonic stem cells was confirmed by Southern blot analysis, and the cells were injected into C57BL/6N blastocysts. To obtain *Sik3*-deficient embryos, *Sik3* heterozygous male and female mice were mated and WT littermates were used as controls. *Per2-luc*$^{+}$ mice were originally generated by Joseph Takahashi (Yoo et al., 2004). All mice used in the experiments were mated with C57BL/6J mice (SLC Japan). Genotyping was performed using genomic DNA from a tail tip of each mouse via a standard protocol as previously described (Sasagawa et al., 2012; Yoo et al., 2004).

Behavioral analyses

Mice were individually housed in translucent polypropylene cages under 12:12 LD (200 lux) and DD conditions, and locomotor activity was assessed by an area sensor (infrared sensor, Omron). Activity was continuously monitored and analyzed using ClockLab software (Actimetrics).

In situ hybridization

Riboprobe was labeled with ^{35}S-UTP (Amersham/GE Healthcare) by *in vitro* transcription using either T7 or SP6 polymerase (Promega). Frozen mouse brain sections (40 μm thick) were hybridized with riboprobe overnight, and exposed to Kodak film (BioMax MR). The *Sik3* cDNA (550 bp) was amplified via PCR and subcloned into a pGEM-T Easy Vector (Promega). The plasmids were linearized with NcoI to synthesize riboprobe.

Immunohistochemistry

Under deep pentobarbital anesthesia (100 mg/kg body weight, i.p.), mice were fixed transcardially with 4% paraformaldehyde in 0.1 M sodium phosphate buffer (PB, pH 7.2), and frozen sections (30 μm thick) were prepared. Immunohistochemical incubations were performed at 4 °C for 4 overnights using phosphate-buffered saline (PBS, pH 7.2) containing 0.1% TritonX-100 (PBS-T) with 5% skim milk (Nacalai). For immunofluorescence, sections were incubated in a free-floating state with a mixture of primary antibodies for 4 overnights (1 μg/ml), then Alexa Fluor-488 anti-rabbit secondary antibody (1:200, Invitrogen; Jackson ImmunoResearch) overnight at 4 °C. For immunohistochemical analysis, we used affinity-purified primary SIK3 antibody (BD Bioscience).

Bioluminescence measurement, imaging, and quantitative analysis

For bioluminescence recording, NIH3T3 cell lines (Riken Cell Bank) transfected

with *Bmal1-luc* were used. For SCN imaging, adult *Sik3*-/- *Per2-luc*$^{+/+}$ and *Sik3*$^{+/+}$ *Per2-luc*$^{+/+}$ mice were used. Cells were harvested in a 35-mm petri dish with DMEM culture medium including 10% fetal calf serum (FCS), 100 nM DEX, and 0.1 mM luciferin, and circadian bioluminescence rhythm was monitored in Kronos (ATTO). For single-cell time-lapse imaging, LV 200 (Olympus) was used for cultured cells or SCN slices. SCN slices from adult *Sik3*$^{-/-}$ *Per2-luc*$^{+/+}$ and *Sik3*$^{+/+}$ *Per2-luc*$^{+/+}$ mice were prepared using a Microslicer (Dosaka Japan, 300 μm thick) and incubated on MilliCell membrane (Merck Millipore) in a 35-mm petri dish with culture medium (DEM-F12 supplemented with B27, Life Technologies). Exposure time for a single image was 55 min, and time-lapse images were captured for 5 consecutive days. Movies were produced using MetaMorph software (Molecular Devices).

Analysis of period and acrophase in SCN slices

For each pixel of the bioluminescence movie, the time series was extracted. Each data-set was detrended and analyzed via the chi-square periodogram (Sokolove and Bushell, 1978). Only periods with a significance level of less than 10% were plotted (Fig. 2). The acrophase was subsequently computed via Cosinor's method (Halberg, 1967), which extracts a peak phase of the bioluminescence signal of each pixel. Each pixel's phase relative to that of the averaged signal over the whole SCN slice was plotted (Fig. 2).

Cell culture and plasmids for transfection

NIH3T3 and HEK293T17 cells were cultured and passaged under 5% CO_2 in DMEM (Sigma) containing 1.8 mg/ml $NaHCO_3$, 4.5 mg/ml glucose, 100 U/ml penicillin, 100 μg/ml streptomycin, and 10% FCS (Equitech Bio, Inc.). NIH3T3 and HEK293T17 cells were transiently transfected using Lipofectamine Plus reagent (Invitrogen) and Lipofectamine 2000 reagent (Invitrogen) respectively, in accordance with the manufacturer's instructions. The pEGFP-C1 plasmid (Clontech) was used as a transfection control. A vector encoding 6xMyc epitope-tagged PER2 (termed myc-PER2 in the figures) was kindly provided by Dr. Louis Ptacek (University of California, San Francisco). For Flag-SIK3, an oligonucleotide encoding the FLAG epitope sequence was fused to the 5'-end of full-length mouse *Sik3* (m*Sik3*) cDNA cloned into pcDNA 3.1. Mutations (Lys to Met at K37 or Thr to Glu at T163) were introduced into *mSik3* using site-directed mutagenesis. Flag-CKIε and Flag-CKIε−KN (Kinase Negative) have been described previously (Doi et al., 2004). Several shRNA expression vectors targeting m*Sik3* gene and a control vector were obtained from QIAGEN. The following sequences were used: *mSik3* sh#1 (5'- CTGCA GGCAC AAGTG GATGA A-3'), *mSik3* sh#2 (5'- AGCAG CAACC CGAGA ACTGT T-3'), *mSik3* sh#3 (5'- CCCAA CTTTG ACAGG TTAAT A-3'), *mSik3* sh#4 (5'- TGCCA CCACG TTCAG TAGAA A-3'), and control sh (5'- GGAAT CTCAT TCGAT GCATA C-3'). The target sequences were inserted into a pGeneClip neomycin vector (Promega).

Immunoblotting

Proteins separated by SDS-PAGE were transferred to polyvinylidene difluoride

membrane (Millipore). The blots were blocked in a blocking solution (1% [w/v] skim milk in PBS-T [50 mM Tris-HCl, 140 mM NaCl, 1 mM $MgCl_2$; pH 7.4]) for 1 h at 37 °C then incubated overnight at 4 °C with a primary antibody in the blocking solution. Signals were visualized via an enhanced chemiluminescence detection system (PerkinElmer Life Science). The blot membrane was subjected to densitometric scanning, and the band intensities were quantified using Image Quant software (GE Healthcare). The primary antibodies used were anti-β-actin (Sigma), anti-Flag (Sigma), anti-myc (Santa Cruz Biotechnology), anti-GFP (Santa Cruz Biotechnology), and anti-PER2 (Alpha Diagnostic Inc.). Primary antibodies were detected by horseradish peroxidase-conjugated anti-rabbit or anti-mouse IgG (Kirkegaard and Perry Laboratories).

Immunoprecipitation

Transfected cells were lysed for 30 min in ice-chilled immunoprecipitation (IP) buffer (20 mM HEPES-NaOH, 137 mM NaCl, 2 mM EDTA, 10% [v/v] glycerol, 1% [v/v] Triton X-100, 1 mM DTT, 4 μg/ml aprotinin, 4 μg/ml leupeptin, 50 mM NaF, 1 mM Na_3VO_4, 1 mM phenylmethylsulfonyl fluoride; pH 7.8). The lysate was incubated with the precipitating antibody for 2 h at room temperature or overnight at 4 °C, followed by incubation with 20 μl Protein G-Sepharose beads (GE Healthcare) for 2 h at 4 °C. Beads were washed three times with IP buffer and subjected to immunoblotting.

Degradation assay

NIH3T3 cells were transfected with myc-PER2 and Flag-SIK3 expression vectors or *Sik3*-KD vectors, and cultured for 48 h. The transfected cells were then treated with cycloheximide (Nakalai tesque; final concentration, 100 μg/ml) for the time periods specified in the figures Fig. 3, Supplementary Fig. 4), and then harvested, followed by immunoblotting.

PPase assay

NIH3T3 cells were transfected with myc-PER2 and Flag-SIK3 expression vectors or *Sik3*-KD vectors, and cultured for 48 h. Immunoprecipitated myc-PER2 were incubated with 400 IU λPPase (Sigma) in Lambda Protein Phosphatase Buffer (Sigma) containing 2 mM $MnCl_2$ for 30 min at 30 °C.

***In vitro* kinase assay**

NIH3T3 cells were transfected with myc-PER2 vector and cultured for 48 h. Immunoprecipitated myc-PER2 were incubated with GST-tagged recombinant human SIK3 (aa.1–307) (SignalChem) in kinase assay buffer (50 mM Tris-HCl, 10 mM $MgCl_2$, 100 mM NaCl, 1 mM DTT, 10% glycerol, 1 mM ATP; pH 7.4) at 30 °C for 30 min or 75 min.

Statistics

All data are expressed as the mean ± SEM or SD. Statistical significance was evaluated via Student's *t*-test, and was set at the $p < 0.05$ level. One-way ANOVA

followed by Dunnett's test or Turkey's test was used for multiple comparisons. For Figures 1f, 2i, and 2j, tests for equality of variance (F-test) were performed, and statistical significance was set at the $p < 0.05$ level.